Title
Reduction of motion artifacts in carotid MRI using free-induction decay navigators

Journal
Journal of Magnetic Resonance Imaging, 40(1)

ISSN
1053-1807

Authors
Dyverfeldt, Petter
Deshpande, Vibhas S
Kober, Tobias
et al.

Publication Date
2014-07-01

DOI
10.1002/jmri.24389

Peer reviewed

Published in final edited form as:
J Magn Reson Imaging. 2014 July ; 40(1): 214–220. doi:10.1002/jmri.24389.

Reduction of Motion Artifacts in Carotid MRI using FID Navigators

Petter Dyverfeldt, PhD[1], **Vibhas S Deshpande, PhD**[2], **Tobias Kober, PhD**[3], **Gunnar Krueger, PhD**[3], and **David Saloner, PhD**[1,4]

[1]Department of Radiology & Biomedical Imaging, University of California San Francisco, San Francisco, CA, United States [2]Siemens Medical Solutions USA, Inc., San Francisco, CA, United States [3]Advanced Clinical Imaging Technology, Siemens Healthcare Sector IM S AW, Lausanne, Switzerland [4]Veterans Affairs Medical Center, San Francisco, CA, United States

Abstract

Purpose—To develop a framework for prospective free-induction decay (FID) based navigator gating for suppression of motion artifacts in carotid MRI and to assess its capability in-vivo.

Methods—An FID-navigator, comprising a spatially-selective low flip-angle sinc-pulse followed by an ADC-readout, was added to a conventional turbo spin-echo (TSE) sequence. Real-time navigator processing delivered accept/reject-and-reacquire decisions to the sequence. In this IRB-approved study, seven volunteers were scanned with a 2D T2-weighted TSE sequence. A reference scan with volunteers instructed to minimize motion as well as non-gated and gated scans with volunteers instructed to perform different motion tasks were performed in each subject. Multiple image quality measures were employed to quantify the effect of gating.

Results—There was no significant difference in lumen-to-wall sharpness (2.3±0.3 vs. 2.3±0.4), contrast-to-noise ratio (CNR) (9.0±2.0 vs. 8.5±2.0) or image quality score (3.1±0.9 vs. 2.6±1.2) between the reference and gated images. For images acquired during motion, all image quality measures were higher ($p < 0.05$) in the gated compared to non-gated images (Sharpness: 2.3±0.4 vs. 1.8±0.5, CNR: 8.5±2.0 vs. 7.2±2.0, score: 2.6±1.2 vs. 1.8±1.0).

Conclusion—Artifacts caused by the employed motion tasks deteriorated image quality in the non-gated scans. These artifacts were alleviated with the proposed FID-navigator.

Keywords

Carotid MRI; Motion Compensation; FID Navigator; Motion Suppression; Carotid Artery Disease; Atherosclerosis

Correspondence: Petter Dyverfeldt, IMH/KVM, Main Bldg, Floor 12, Linköping University Hospital, 581 83 Linköping, Sweden. petter.dyverfeldt@liu.se, phone: +46 10 1033353.

INTRODUCTION

The current standard approach to the assessment of the risk of stroke due to atherosclerotic carotid disease is based on the degree of luminal stenosis using ultrasound (1). However, especially in asymptomatic individuals, the ability of the degree of stenosis to predict the risk of thromboembolic events is uncertain (2). In advanced stages of carotid atherosclerosis, thromboemboli from atheroma at the carotid bifurcation can obstruct distal vessels in the brain. In the western world, emboli from extracranial carotid plaque are estimated to be the cause of 25% of all strokes (3). It is therefore of high importance to be able to evaluate not only lumenal irregularities but also the geometric and compositional morphology of the vessel wall. Better strategies for detecting patients at risk of thromboembolic events from atherosclerotic plaques are needed (4).

MRI offers several opportunities for evaluation of atherosclerotic plaques in the carotid arteries (5,6). The excellent soft-tissue contrast provided by MRI permits determination of compositional and morphological features of plaques. Specifically, imaging based on contrast-weighted turbo-spin echo (TSE) sequences has been shown capable of quantification of major plaque components with histology as a reference (7–9). The capability of MR plaque imaging has been further augmented by the introduction of dedicated carotid coils and blood-suppression techniques (10–20). However, carotid MRI is severely hampered by motion-related image artifacts. For example, a recent carotid MRI multicenter trial reported that 15% of the scans had unacceptable image quality due to motion (21). Previous efforts directed at reducing motion artifacts in carotid MRI include mono-directional approaches such as conventional 1D navigator gating with the navigator positioned over the epiglottis, and 1D self-gating where motion detection is based on cross-correlation between projections of the image slab (22–24). Another approach involves the use of a dedicated coil designed to detect swallowing motion at the laryngeal prominence (25).

These previous approaches have primarily targeted swallowing. However, motion-artifacts in the neck can also be caused by a variety of other sources including, coughing, chewing, breathing, and bulk motion. Furthermore, the motion is typically non-rigid and not limited to a single direction (26). FID navigators, which monitor the center of k-space without any spatial encoding, represent an approach to motion-detection that is sensitive to motion in all directions (27,28). FID navigators can be combined with virtually any sequence and impose little or no scan time penalty. For example, FID navigator gating was recently shown to permit motion-correction in brain imaging (28,29).

The objective of the present study was to develop a framework for prospective free-induction decay (FID) based navigator gating for suppression of motion artifacts in carotid MRI and to assess its capability in-vivo

MATERIALS AND METHODS

A prospective FID-navigator was implemented in a conventional TSE sequence. Real-time navigator processing delivered accept/reject-and-reacquire decisions to the sequence and

visual feedback to the scanner user-interface. Validation of the ability of this gating technique to reduce motion artifacts was performed in-vivo.

FID navigator

The present FID-navigator comprises its own radio-frequency excitation, which is achieved by a spatially-selective 15-degree flip-angle sinc-pulse. The slab-selective excitation is followed by analogue-to-digital converter (ADC) recording in absence of gradients. The total duration of each instance (excitation + ADC) of the FID navigator is 950 μs. By having its own excitation, the FID-navigator can be applied outside of each excitation/readout block of the host sequence and thereby does not interfere with timing and contrast characteristics. In this study, this stand-alone FID navigator was added prior to each 90 degree excitation pulse in a conventional turbo spin-echo (TSE) sequence.

Real-time navigator processing was implemented online to deliver accept/reject-and-reacquire decisions to the sequence as well as visual feedback to the scanner's user interface (Figure 1). The signal processing used here is based on that described by Kober et al (28) and was adjusted to provide robust motion compensation for carotid imaging. For each instance of the FID navigator, one complex data point per channel is calculated by taking the average of the last 50% of the complex FID signal. In the current implementation, 128 complex FID points are used. The first three TRs are ignored to let the system stabilize. The following five TRs constitute a learning phase during which a complex reference data point for each coil element is recorded.

After the initial learning phase, each incoming complex data point is compared with the complex reference data point so as to obtain the following raw FID navigator signal (RawNavSignal):

$$\mathrm{RawNavSignal}(n)=\frac{1}{N_{\mathrm{C}}}\sum_{i=1}^{N_{\mathrm{C}}}\frac{|\mathrm{nav}_i(n)-\mathrm{ref}_i|}{|\mathrm{ref}_i|}$$

where n denotes the n^{th} navigator signal, N_c is the number of coil elements and $nav_i(n)$ is the complex data point of coil element i of the n^{th} navigator signal. As described in Kober et al, the FID signal is affected by system instabilities (28). Our preliminary investigations with carotid applications indicated that the baseline FID signal can also be altered by subject-based factors. Such drift has been observed previously and may be caused by involuntary muscle relaxation (30). To avoid low gating-efficiency due to low-frequency signal alterations, a drift corrected navigator signal (CorrNavSignal) is calculated by subtracting the median value of the most recently accepted RawNavSignals from the current RawNavSignal (see Figure 2). This drift estimation is based on accepted RawNavSignals not older than eight TRs. If the number of accepted data points within that period of time is small ($n < 4$), the lowest values of the non-accepted RawNavSignal are used to support the drift estimation.

Motion detection is performed with the CorrNavSignal. A dynamic gating threshold is calculated as three standard deviations of up to 25 of the previously accepted

CorrNavSignals. If the incoming CorrNavSignal exceeds the threshold the corresponding imaging data is rejected and re-acquired in the subsequent TR. The time course of the CorrNavSignal is also fed back to the scanner user-interface for real-time visual feedback.

The present FID navigator has its own excitation and can thus be oriented independently of the host sequence. The orientation and spatial extent of the excitation slab used for FID-gating was implemented to be adjustable on the scanner user-interface. The FID signal represents the sum of the transverse magnetization of all excited spins and the navigator slab was positioned accordingly. In the present study, a sagittal slab orientation was used to avoid contamination of otherwise strong signal contributions from regions adjacent to the surface coil arrays. The slab was positioned between the carotid arteries to avoid any spin-history artifacts in the TSE images. The localized sensitivity of the surface coil used here minimized contributions from the chest which might otherwise over-emphasize FID signal alterations caused by breathing.

In-Vivo Study

To evaluate feasibility, 7 normal volunteers (age: 22–63 years, mean age: 33 years, 3 female) were scanned with a finger-pulse gated fat-saturated 2D T2-weighted TSE sequence (pixel size 0.5×0.5 mm^2, matrix size 704×704, slice thickness 2 mm, TE = 61 ms, TR = 2 cardiac cycles, bandwidth = 230 Hz/pixel, echo train length = 15) on a 1.5T Siemens Avanto scanner equipped with a custom-built 8-element carotid coil. The institutional review board approved the study and informed consent was obtained from all subjects. Subjects were placed in the supine position with their heads resting in a plastic support that is shaped to the posterior third of the head. The support is covered with foam padding to avoid discomfort. A trigger delay was used to direct image acquisition to diastole. Saturation bands were used to suppress the signal of inflowing blood. Phase-encoding was in the anterior-to-posterior direction. The current implementation did not support signal averaging which is commonly used to obtain adequate signal-to-noise ratio in carotid MRI. As a substitute for averaging we employed a large field-of-view (360×360 mm^2) necessitating a large number of phase-encodes (which accounts for the large matrix size). Nominal scan time was about 1 minute and 30 seconds.

With a fixed slice location 5 mm proximal to the carotid bifurcation, the following five scans were performed in randomized order:

- Reference scan (non-gated) with volunteers instructed to abstain from swallowing and breathe shallowly
- Non-gated and gated scans with volunteers instructed to swallow at 20, 40, 50 60, and 80% of the scan
- Non-gated and gated scans with volunteers instructed to take quick deep breaths at 20, 40, 50 60, and 80% of the scan

Both the left and right common carotid arteries (CCA’s) were considered in the subsequent analysis. FID navigator signals were recorded also for the reference and non-gated scans.

Data Analysis

Qualitative image quality assessment was performed by two blinded reviewers (PD and DS) with 3 and 20 years of experience in carotid MRI, respectively. The reviewers graded image quality on separate sittings and the images were presented in a randomized fashion. Each image was graded based on the quality of the bilateral CCA vessel wall depiction. The following five-point scale was used: 0 = very poor wall delineation, 1 = incomplete wall delineation and severe boundary blurring, 2 = moderate wall delineation and appreciable boundary blurring at some locations, 3 = good wall delineation and minor boundary blurring at some locations, 4 = excellent wall delineation and little or no boundary blurring. All analysis was performed on values averaged between the two observers.

Quantitative image quality assessment was performed by measuring the sharpness of the lumen-to-wall interface and the contrast-to-noise ratio between the vessel wall and lumen. Additionally, wall area was measured to assess the effects of gating on this commonly used morphological parameter. Sharpness was measured as described in (31); images were upsampled four-fold with bilinear interpolation and image intensity profiles were generated along four select lines that perpendicularly traversed the vessel wall at four different locations. Manual registration was used to match the four lines between the different images acquired in each subject. The 20 and 80% points between the maximum wall signal intensity and the lumen signal intensity were identified on the signal intensity profiles. Sharpness was calculated as the reciprocal of the distance between the points. Distance was averaged over all the four locations in each CCA.

The ordinal image scores for the reference, gated, and non-gated scans were compared using a paired two-tailed Wilcoxon signed rank test. The lumen-to-wall sharpness, CNR, and wall area for the reference, gated, and non-gated scans were compared using a paired two-tailed Student’s t-test.

Additionally, the effects of swallowing vs. breathing were compared using all image quality metrics. The total number of observations used in the image quality score evaluation was 7 for each motion task (no motion, swallowing, or breathing). For the lumen-to-wall sharpness, CNR and wall area analysis, the corresponding number was 14 as each CCA was considered individually. *P*-values less than 0.05 were considered to be statistically significant.

RESULTS

Data were acquired successfully in all subjects. Although motion instructions were given in a consistent way for all scans, substantial differences in the FID navigator signals were observed both on an inter- and intra-subject basis. This is exemplified in Figure 3 where CorrNavSignal time courses and corresponding T2w TSE images are shown for reference, non-gated (breathing) and gated (breathing) data acquired in one subject. Although the CorrNavSignals indicate that motion did occur at the instructed time points, the effect of motion on the FID signal varies during each scan. Also, when compared to the FID signal time courses shown in Figure 2, the motion tasks are less well visualized in Figure 3. This may largely be attributed to variations in actual motion as well as timing of motion relative

to the timing of the navigator. Nevertheless, the successful alleviation of motion effects with gating can be appreciated in the reconstructed images.

Results from the image quality score, lumen-to-wall sharpness, CNR, and wall area analyses are summarized in Figure 4, Table 1, and Table 2. For images acquired during motion, the image quality score, lumen-to-wall sharpness, and CNR were significantly higher in the gated compared to non-gated images ($p < 0.05$). Wall area was smaller in the gated compared to non-gated images ($p < 0.05$). None of the image quality metrics differed between the reference and gated images (Table 1 and Table 2).

Assessment of the respective effects of swallowing and breathing showed that there was no difference between swallowing and breathing in the non-gated images. Additionally, there was no difference between reference and gated images for any of the two motion events. Image quality appeared to be higher in the reference and gated compared to non-gated images for swallowing alone and for breathing alone, although these differences did not reach statistically significant levels for all image quality metrics in this small-sample (n=7) study.

DISCUSSION

Multicontrast-weighted TSE imaging has well documented potential for quantifying plaque components and improving risk-stratification of carotid atherosclerosis (7–9,32). However, a large number of scans have unacceptable image quality due to motion (21). This study described a novel approach to motion compensated carotid MRI and validated its capability to reduce motion artifacts in contrast-weighted carotid MRI in-vivo. Image quality was significantly higher in gated compared to non-gated images acquired during motion and there was no difference between gated images and reference images acquired with subjects instructed to breathe shallowly and not to swallow. The proposed FID navigator might be expected to reduce the currently high failure rate of MR imaging of the carotid arteries and provides a step in taking carotid MRI towards greater clinical use.

By applying the FID-navigator's low flip-angle RF pulse outside of the host sequence (TSE), the present FID-navigator does not affect its timing and contrast characteristics. The total duration of the navigator is less than 1ms, and it will thus only slightly affect the efficiency of multislice and 3D applications. The proposed FID navigator is not limited to TSE sequences. With its stand-alone configuration, it can readily be implemented in virtually any sequence that would benefit from motion compensation capabilities.

Effects of swallowing and breathing on the recorded FID signal were noted to vary not only between subjects but also within a given scan. This may in part be explained by the fact that the FID signal was recorded in less than 1 ms on every 2nd heartbeat. The most pronounced part of a given motion event may have occurred outside of this short period of time. While motion may in some cases have been initiated during the TSE echo-train, the successful alleviation of motion artifacts with gating suggests that the FID navigator successfully detected the motion experienced by the host sequence. This is well in line with a recent

study on carotid MRI with 1D self-gating, which demonstrated successful detection of swallowing motion also in SPACE imaging with long echo-trains (24).

While most of the previous efforts directed at reducing motion artifacts have targeted swallowing, several sources of motion impact image quality in carotid MRI. Others have demonstrated that one such source of image artifacts is breathing (26,30). This was confirmed in the present study where little difference in image quality was seen in the non-gated images acquired during breathing and swallowing. The proposed FID navigator appears capable of handling both types of motion.

The in-vivo experiments reported here were performed with a custom-built 8-element dual phased-array receiver. The arrays were positioned at the left and right side of the neck, respectively, so as to maximize signal from the carotid bifurcation. The localized sensitivity of this phased-array receiver resulted in very small signal contributions from the chest. A different coil configuration, such as a conventional neck coil, may register more signal from the upper part of the chest. This, in turn, may result in more pronounced breathing-related alterations of the FID navigator signal. Further investigations are needed to establish the effect of different coil configurations on FID navigator gating.

Limitations of this study include the lack of patient data acquired under typical conditions. Our study participants were instructed to perform specific motion (swallowing and breathing) tasks so as to validate the capability of FID-gating. Although these motion events are well representative of motion that affects carotid MRI, further studies are needed to evaluate the sensitivity of the FID navigator to other types of motion. Patients undergoing carotid MRI are typically instructed to minimize swallowing and to lie as still as possible. Larger-scale studies with patients given such conventional instructions could determine the degree of improvement that FID navigator gating has to offer in a clinical setting. A challenging aspect of FID navigator gating is that the baseline level of the FID signal can be altered during the scan. Such low-frequency signal alterations can be caused both by system-induced drift and physiological factors such as involuntary muscle relaxation and changes in jaw position. Kober and colleagues addressed this challenge by measuring the system-induced drift and used that information to define a maximum acceptable slope in the drift estimation (28). The drift compensation used in the present study provided a robust gating signal and ensured that the scan would always finish. At the same time, the present approach is likely to accept more motion (28). For example, a change of head position would result in an altered FID baseline level. Such motion could lead to an aborted scan with a drift-restricted approach but would, eventually, be accepted with the present approach. This may be addressed by having such an event trigger a user-interface prompt that recommends a re-start of the scan. A more efficient way to deal with such motion may be to combine drift-restriction with registration-based bulk motion correction. Acquisition of low-resolution image data for such bulk-motion compensation could be triggered when the accumulated number of rejected navigator signals reaches a certain threshold. The performance of this approach in subjects other than healthy volunteers will be explored in a future study in the clinical setting on patients with vascular disease.

In conclusion, the proposed prospective FID navigator reduces motion artifacts in carotid MRI. This can be expected to reduce the currently high failure rate of carotid MRI.

Acknowledgments

Grant sponsors: Fulbright Commission (PD), Swedish Heart-Lung Foundation (PD), Swedish Brain Foundation (PD), NS059944 from the NIH (DS) and a VA MERIT Review Grant (DS).

The authors acknowledge XXX for constructive comments on the manuscript.

References

1. Goldstein LB, Bushnell CD, Adams RJ, et al. Guidelines for the Primary Prevention of Stroke A Guideline for Healthcare Professionals From the American Heart Association/American Stroke Association. Stroke. 2011; 42(2):517–584. [PubMed: 21127304]
2. Gates PC, Chambers B, Yan B, Chong W, Denton M. Symptomatic and asymptomatic carotid stenosis: just when we thought we had all the answers. Intern Med J. 2006; 36(7):445–451. [PubMed: 16780451]
3. Timsit SG, Sacco RL, Mohr JP, et al. Early clinical differentiation of cerebral infarction from severe atherosclerotic stenosis and cardioembolism. Stroke. 1992; 23(4):486–491. [PubMed: 1561677]
4. Naghavi M, Libby P, Falk E, et al. From vulnerable plaque to vulnerable patient: a call for new definitions and risk assessment strategies: Part I. Circulation. 2003; 108(14):1664–1672. [PubMed: 14530185]
5. Saloner D, Acevedo-Bolton G, Wintermark M, Rapp JH. MRI of geometric and compositional features of vulnerable carotid plaque. Stroke. 2007; 38(2 Suppl):637–641. [PubMed: 17261706]
6. Saam T, Hatsukami TS, Takaya N, et al. The vulnerable, or high-risk, atherosclerotic plaque: noninvasive MR imaging for characterization and assessment. Radiology. 2007; 244(1):64–77. [PubMed: 17581895]
7. Serfaty JM, Chaabane L, Tabib A, Chevallier JM, Briguet A, Douek PC. Atherosclerotic plaques: classification and characterization with T2-weighted high-spatial-resolution MR imaging-- an in vitro study. Radiology. 2001; 219(2):403–410. [PubMed: 11323464]
8. Clarke SE, Hammond RR, Mitchell JR, Rutt BK. Quantitative assessment of carotid plaque composition using multicontrast MRI and registered histology. Magn Reson Med. 2003; 50(6): 1199–1208. [PubMed: 14648567]
9. Saam T, Ferguson MS, Yarnykh VL, et al. Quantitative Evaluation of Carotid Plaque Composition by In Vivo MRI. Arteriosclerosis, Thrombosis, and Vascular Biology. 2005; 25(1):234–239.
10. Hayes CE, Mathis CM, Yuan C. Surface coil phased arrays for high-resolution imaging of the carotid arteries. Journal of Magnetic Resonance Imaging. 1996; 6(1):109–112. [PubMed: 8851414]
11. Song HK, Wright AC, Wolf RL, Wehrli FW. Multislice double inversion pulse sequence for efficient black-blood MRI. Magnetic Resonance in Medicine. 2002; 47(3):616–620. [PubMed: 11870851]
12. Parker DL, Goodrich KC, Masiker M, Tsuruda JS, Katzman GL. Improved efficiency in double-inversion fast spin-echo imaging. Magnetic Resonance in Medicine. 2002; 47(5):1017–1021. [PubMed: 11979583]
13. Yarnykh VL, Yuan C. Multislice double inversion-recovery black-blood imaging with simultaneous slice reinversion. Journal of Magnetic Resonance Imaging. 2003; 17(4):478–483. [PubMed: 12655588]
14. Itskovich VV, Mani V, Mizsei G, et al. Parallel and nonparallel simultaneous multislice black-blood double inversion recovery techniques for vessel wall imaging. Journal of Magnetic Resonance Imaging. 2004; 19(4):459–467. [PubMed: 15065170]
15. Hinton DP, Cury RC, Chan RC, et al. Bright and black blood imaging of the carotid bifurcation at 3. 0T. European Journal of Radiology Cardiac Imaging. 2006; 57(3):403–411.

16. Koktzoglou I, Li D. Diffusion-Prepared Segmented Steady-State Free Precession: Application to 3D Black-Blood Cardiovascular Magnetic Resonance of the Thoracic Aorta and Carotid Artery Walls. Journal of Cardiovascular Magnetic Resonance. 2007; 9(1):33–42. [PubMed: 17178678]
17. Wang J, Yarnykh VL, Hatsukami T, Chu B, Balu N, Yuan C. Improved suppression of plaque-mimicking artifacts in black-blood carotid atherosclerosis imaging using a multislice motion-sensitized driven-equilibrium (MSDE) turbo spin-echo (TSE) sequence. Magnetic Resonance in Medicine. 2007; 58(5):973–981. [PubMed: 17969103]
18. Makhijani MK, Hu HH, Pohost GM, Nayak KS. Improved blood suppression in three-dimensional (3D) fast spin-echo (FSE) vessel wall imaging using a combination of double inversion-recovery (DIR) and diffusion sensitizing gradient (DSG) preparations. Journal of Magnetic Resonance Imaging. 2010; 31(2):398–405. [PubMed: 20099353]
19. Fan Z, Zhang Z, Chung YC, et al. Carotid arterial wall MRI at 3T using 3D variable-flip-angle turbo spin-echo (TSE) with flow-sensitive dephasing (FSD). Journal of Magnetic Resonance Imaging. 2010; 31(3):645–654. [PubMed: 20187208]
20. Balu N, Yarnykh VL, Scholnick J, Chu B, Yuan C, Hayes C. Improvements in carotid plaque imaging using a new eight-element phased array coil at 3T. Journal of Magnetic Resonance Imaging. 2009; 30(5):1209–1214. [PubMed: 19780187]
21. Boussel L, Arora S, Rapp J, et al. Atherosclerotic Plaque Progression in Carotid Arteries: Monitoring with High-Spatial-Resolution MR Imaging - Multicenter Trial. Radiology. 2009; 252(3):789–796. [PubMed: 19508991]
22. Crowe LA, Keegan J, Gatehouse PD, et al. 3D volume-selective turbo spin echo for carotid artery wall imaging with navigator detection of swallowing. Journal of Magnetic Resonance Imaging. 2005; 22(4):583–588. [PubMed: 16161101]
23. Koktzoglou I, Li D. Submillimeter isotropic resolution carotid wall MRI with swallowing compensation: imaging results and semiautomated wall morphometry. Journal of magnetic resonance imaging. 2007; 25(4):815–823. [PubMed: 17345637]
24. Fan Z, Zuehlsdorff S, Liu X, Li D. Prospective self-gating for swallowing motion: a feasibility study in carotid artery wall MRI using three-dimensional variable-flip-angle turbo spin-echo. Magn Reson Med. 2012; 67(2):490–498. [PubMed: 22161627]
25. Chan CF, Gatehouse PD, Hughes R, Roughton M, Pennell DJ, Firmin DN. Novel technique used to detect swallowing in volume-selective turbo spin-echo (TSE) for carotid artery wall imaging. Journal of Magnetic Resonance Imaging. 2009; 29(1):211–216. [PubMed: 19097078]
26. Boussel L, Herigault G, De La Vega A, Nonent M, Douek PC, Serfaty JM. Swallowing, arterial pulsation, and breathing induce motion artifacts in carotid artery MRI. Journal of Magnetic Resonance Imaging. 2006; 23(3):413–415. [PubMed: 16463340]
27. Brau A, Brittain JH. Generalized self-navigated motion detection technique: Preliminary investigation in abdominal imaging. Magnetic resonance in medicine. 2006; 55(2):263–270. [PubMed: 16408272]
28. Kober T, Marques JP, Gruetter R, Krueger G. Head motion detection using FID navigators. Magnetic Resonance in Medicine. 2011; 66(1):135–143. [PubMed: 21337424]
29. Kober T, Gruetter R, Krueger G. Prospective and retrospective motion correction in diffusion magnetic resonance imaging of the human brain. NeuroImage. 2012; 59(1):389–398. [PubMed: 21763773]
30. Chan, CF.; Gatehouse, PD.; Pennell, DJ.; Firmin, DN. The potential problems associated with carotid motion in carotid artery imaging. Proc Intl Soc Mag Reson Med; Honolulu, Hawai'i, USA. 2009.
31. Li D, Carr JC, Shea SM, et al. Coronary arteries: magnetization-prepared contrast-enhanced three-dimensional volume-targeted breath-hold MR angiography. Radiology. 2001; 219(1):270–277. [PubMed: 11274569]
32. Takaya N, Yuan C, Chu B, et al. Association Between Carotid Plaque Characteristics and Subsequent Ischemic Cerebrovascular Events. Stroke. 2006; 37(3):818–823. [PubMed: 16469957]

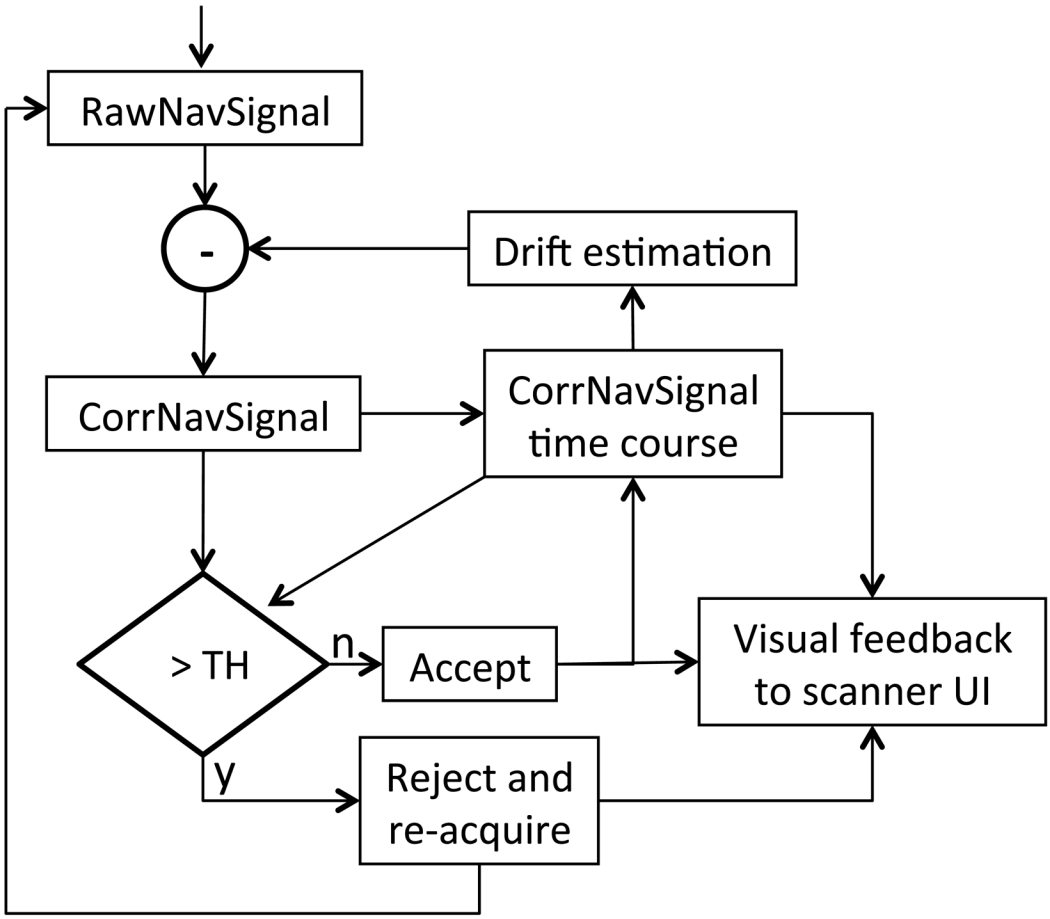

Figure 1.

Schematic of the FID navigator motion detection algorithm. Incoming FID signals from all coil elements are combined to obtain a raw FID navigator (RawNavSignal) signal. Compensation of baseline drift yields a corrected FID navigator (CorrNavSignal) signal which is compared against a dynamic motion-detection threshold. Rejected data points are immediately re-acquired. The accept/reject decisions and the time course of the CorrNavSignal are delivered to the scanner UI for visual feedback.

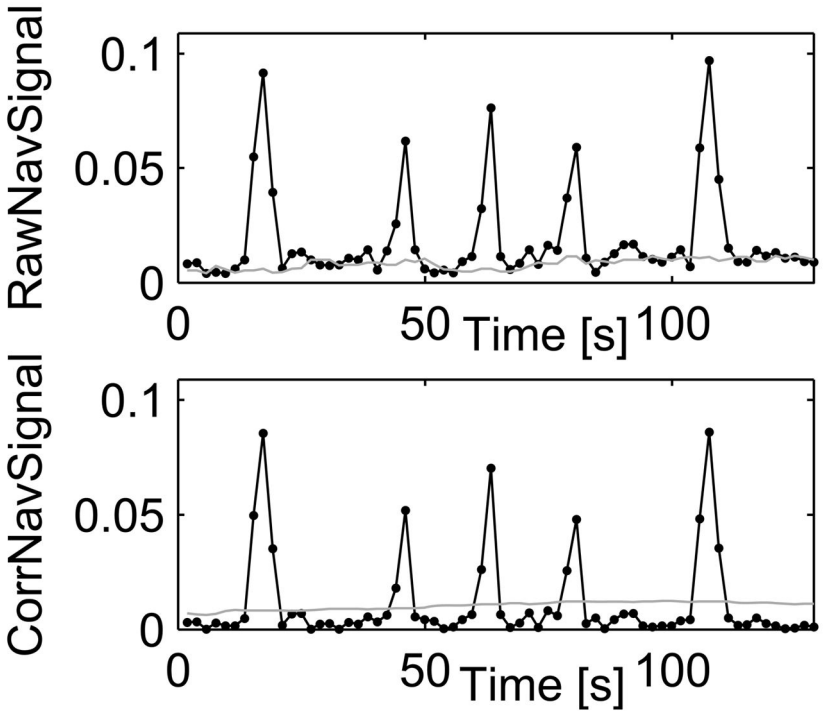

Figure 2.

Example case illustrating the FID navigator signal processing used in this study. In this example, the subject was instructed to take quick deep breaths at five pre-defined time points. **Upper panel:** An uncorrected FID navigator signal (RawNavSignal, solid line with markers) is obtained by comparing each incoming FID signal with a reference signal. Motion distorts the FID signal and is thus reflected by an elevated RawNavSignal. Baseline drift in the RawNavSignal signal is estimated based on previously accepted data points (gray line). **Lower panel**: Gating is performed on the drift-corrected navigator signal (CorrNavSignal, solid line). A threshold (gray line) is calculated based on previously accepted data points.

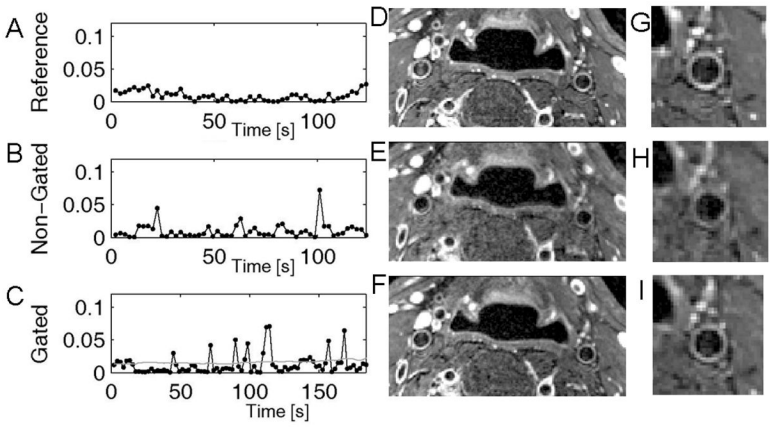

Figure 3.

Navigator signal (A–C) and T2-weighted TSE image (D–I) for reference (top), nongated breathing (middle), and gated breathing (bottom) scans in one subject. The gray line in the panel C indicates the gating threshold. Panels G–I offer zoomed-in views of the left common carotid artery.

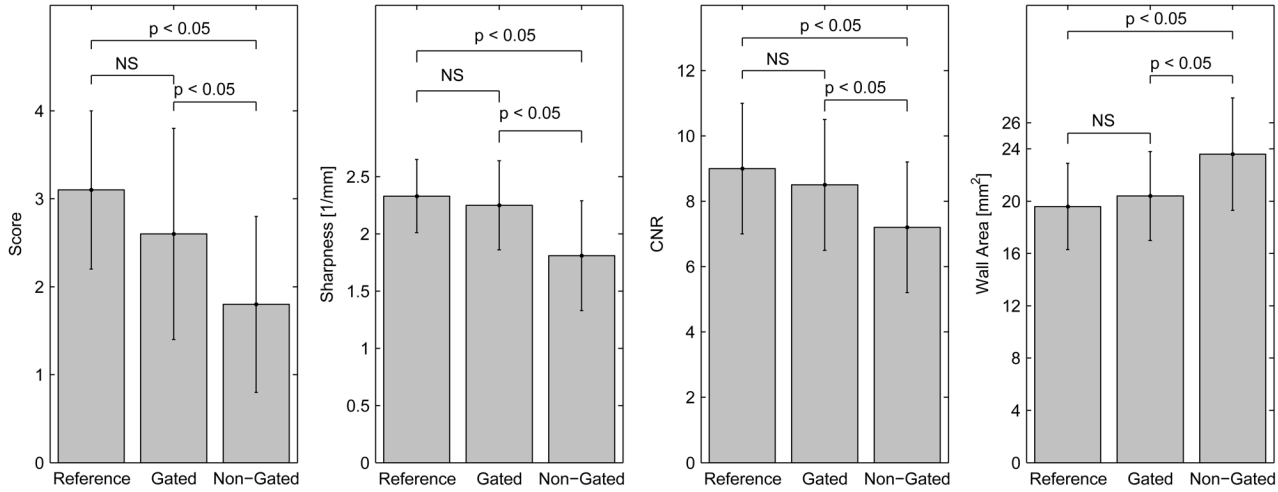

Figure 4.

Illustration of carotid image quality assessment in the Reference, Gated (swallowing and breathing combined), and Non-Gated (swallowing and breathing combined) images. From left to right: Image quality scores, lumen-to-wall sharpness, contrast-to-noise ratio (CNR), and vessel wall area.

Table 1

Mean ± standard deviation of the range of image quality metrics assessed in this study for reference images acquired with subjects instructed to breathe shallowly and not to swallow, gated images acquired with subjects instructed to swallow or take quick deep breaths at predefined instances during the scan, and non-gated images acquired with subjects instructed to swallow or take quick deep breaths at pre-defined instances during the scan.

	Image quality score	Lumen-to-wall sharpness	Contrast-to- noise ratio	Wall area
Reference	3.1 ± 0.9	2.3 ± 0.3	9.0 ± 2.0	19.6 ± 3.3
Gated	2.6 ± 1.2	2.3 ± 0.4	8.5 ± 2.0	20.4 ± 3.5
Non-gated	1.8 ± 1.0	1.8 ± 0.5	7.2 ± 2.0	23.6 ± 4.3
Swallowing, gated	2.5 ± 1.1	2.2 ± 0.4	8.5 ± 2.0	21.2 ± 3.9
Swallowing, non-gated	1.5 ± 0.9	1.8 ± 0.5	7.0 ± 1.7	23.8 ± 4.5
Breathing, gated	2.8 ± 1.3	2.3 ± 0.4	8.4 ± 2.2	19.6 ± 3.1
Breathing, non-gated	2.1 ± 1.1	1.8 ± 0.4	7.3 ± 2.4	23.4 ± 4.4

Table 2

p-values for statistical comparisons between reference images acquired with subjects instructed to breathe shallowly and not to swallow, gated images acquired with subjects instructed to swallow or take quick deep breaths at pre-defined instances during the scan, and non-gated images acquired with subjects instructed to swallow or take quick deep breaths at pre-defined instances during the scan.

	Compared images	p-values
Swallowing and breathing combined	Reference vs. Gated	$P_{score} = 0.218$ $P_{sharpness} = 0.420$ $P_{CNR} = 0.401$ $P_{area} = 0.430$
	Reference vs. Non-gated	$P_{score} < 0.05$ $P_{sharpness} < 0.05$ $P_{CNR} < 0.05$ $P_{area} < 0.05$
	Gated vs. Non-gated	$P_{score} < 0.05$ $P_{sharpness} < 0.05$ $P_{CNR} < 0.05$ $P_{area} < 0.05$
Separate results for swallowing alone and breathing alone	Reference vs. Swallowing, gated	$P_{score} = 0.156$ $P_{sharpness} = 0.249$ $P_{CNR} = 0.576$ $P_{area} = 0.302$
	Reference vs. Swallowing, non-gated	$P_{score} < 0.05$ $P_{sharpness} < 0.05$ $P_{CNR} < 0.05$ $P_{area} < 0.05$
	Swallowing, gated vs. Swallowing, non-gated	$P_{score} = 0.094$ $P_{sharpne\ ss} < 0.05$ $P_{CNR} = 0.052$ $P_{area} = 0.132$
	Reference vs. Breathing, gated	$P_{score} = 0.875$ $P_{sharpness} = 0.892$ $P_{CNR} = 0.589$ $P_{area} = 0.903$
	Swallowing, gated vs. Breathing, gated	$P_{score} = 0.906$ $P_{sharpness} = 0.822$ $P_{CNR} = 0.942$ $P_{area} = 0.283$
	Reference vs. Breathing, non-gated	$P_{score} = 0.188$ $P_{sharpness} < 0.05$ $P_{CNR} = 0.097$ $P_{area} < 0.05$
	Swallowing, non-gated vs. Breathing, non -gated	$P_{score} = 0.312$ $P_{sharpness} = 0.450$ $P_{CNR} = 0.660$ $P_{area} = 0.830$
	Breathing, gated vs. Breathing, non-gated	$P_{score} = 0.125$ $P_{sharpness} < 0.05$ $P_{CNR} = 0.256$ $P_{area} < 0.05$